Egyptian Journal of Chemistry

http://ejchem.journals.ekb.eg/

Functionalized Ilmenite Ores for Improved Photocatalytic Removal of Pb(II) Ions in an Aqueous Solution by Visible Light Irradiation

Ahmed A. Elnazer[*1], Mokhles K. Azer[1], Elzahraa A. Elgohary[2], Hossam A. El Nazer[2], Yasser M. A. Mohamed*[2]

[a]*Geological Sciences Department, National Research Centre, Dokki, Giza, 12622, Egypt*
[b]*Photochemistry Department, National Research Centre, Dokki, Giza, 12622, Egypt.*

Abstract

The efficient removal of heavy metals from water is a critical environmental problem. Photocatalysis is a new and rapidly growing field of research that offers a promising approach. In this study, ilmenite ore (**IL**) samples procured from the Abu Ghalaga area in Egypt were functionalized through a facile process using hydrogen peroxide. Different characteristic techniques were utilized to examine both the physical and chemical properties of all ilmenite samples including XRF, XRD, SEM, EDX, FTIR, and BET. The XRF data of collected ores (**IL** samples) was demonstrated as the major oxides TiO_2 (36.61-39.73 wt%) and Fe_2O_3 (55.04-55.15 wt%). According to XRD, The main mineral in the Abu Ghalaga ilmenite ore samples is ilmenite $Fe(TiO_3)$ ranging from (78% -83%) While the hematite mineral (Fe_2O_3) ranging from (17% - 22%). The photocatalytic efficiencies of the functionalized ilmenite samples (**f-IL**) were investigated for the removal of Pb(II) ions under visible light irradiation in an aqueous solution. All the functionalized ilmenite samples (**f-IL**) samples exhibited higher specific surface area and total pore volume than their source ilmenite ores (**IL**). The **f-IL** samples displayed effective photocatalytic removal of Pb(II) ions compared to the unfunctionalized ones under optimum conditions. The maximum adsorption capacity (qm) recorded was 309.7 mg/g for the **1-f-IL** sample with removal efficiency reaching 97.6% at pH 7, temperature 25 ^oC, and catalyst dosage 20 mg after 60 min irradiation time under visible light. This study highlights the superior photocatalytic efficiency of functionalized ilmenite towards the removal of Pb(II) ions in an aqueous solution under visible irradiation.

Keywords: Ilmenite; Photocatalytic; Pb(II) ions; Visible light irradiation; Pollution; Wastewater treatment.

1. Introduction

Heavy metals and/or organic pollutants in water cause hazardous effects on human health and the environment due to their toxicity [1]. Pb(II) has been recognized as one of the most highly toxic metal ions, which is bio-accumulative, not biodegradable, and exists in natural environments such as water and agricultural land due to anthropogenic activities. Exposure to high levels of Pb(II) ions has harmful effects on humans that can lead to death [2]. Pb(II) ions are found in large amounts in wastewater from several industries such as metallurgy, and electroplating [3]. The most well-known approaches for the removal of Pb(II) from wastewater are chemical precipitation, filtration, ion exchange, and adsorption [4].

The adsorption technique is more favoured by scientists due to its simplicity, low cost, and high efficiency [5]. Different parameters control the adsorption process of heavy metal ions including the adsorbent dosage, the temperature, the contact time, the initial metal ion concentration and the pH of the wastewater medium [6-10]. Previous studies reported the adsorption of Pb(II) ions using titanium dioxide/carbon nanotube nanocomposites [7]. In another study, ZnO, TiO_2, and Al_2O_3 were used as effective Pb(II) sorbents [8]. Furthermore, the adsorption of Pb(II) ions over Fe_3O_4, SnO_2, and TiO_2 nanoparticles surface has been investigated [9].

However, the need for exploring new eco-friendly, inexpensive and more effective adsorbents is highly demanded for wastewater treatment. In this regard, photocatalytic removal of Pb(II) ions over TiO_2 and other photocatalysts has captured the interest of scientists. Titanium dioxide is the most frequently applied semiconductor photocatalyst in photo-induced degradation processes [10,11]. This process is mainly photo-oxidation of Pb(II) ions to form PbO_2 induced by incident light and sensitized by a photocatalyst [12]. Unfortunately, the traditional extraction techniques of pure TiO_2 from its natural ores require harsh reaction conditions, which not only consume energy but also incur higher costs and are unfriendly to the environment [13]. As well, the macro nature associated with ores decreases their efficiency in different applications. Thus, modifying the surface morphology of natural ores using green

*Corresponding author e-mail: nazer42@yahoo.com
Receive Date: 05 October 2023, Revise Date: 22 October 2023, Accept Date: 01 November 2023
DOI: 10.21608/EJCHEM.2023.240946.8716

methods before utilizing them into various advanced applications, such as oxidation and reduction, is a global concern [14].

Ilmenite (IL) is a weakly magnetic black or steel-grey solid with a $FeTiO_3$ composition, which is mined for production of titanium dioxide. This mineral comprises a stoichiometric content of 53% titanium dioxide (TiO_2), although the real TiO_2 content varies between 40% and 65% [15]. In Egypt, the Abu Ghalaga area in the eastern desert is the largest reserve of ilmenite ore, estimated to be around 50 million tons [16].

The petrography of ilmenite ore from Abu Ghalaga region is distinguished into massive ilmenite (>75 vol% Fe–Ti oxides) and semi-massive ilmenite (~40–60 vol% Fe–Ti oxides). Both types contain variable amounts of plagioclase, amphibole, pyroxenes, apatite and sulfides [17]. The Abu Ghalaga Fe–Ti oxides are composed mainly of pure ilmenite or ilmenite containing ex-solved titanomagnetite and titanohematite. Some magnetite, goethite and hematite rich bands were also detected in the ilmenite ore [17].

In continuing to our previous work on developing materials based on TiO_2 and the discovery of their activity towards the detoxification of greenhouse gases such as NOx [18], SOx [19], CO_2 [11] and CO [20] and removal of pollutants in water [21]. In this study, we decided to investigate the functionalization of ilmenite ore and its use in Pb(II) ions detoxification in an aqueous solution. Three samples of natural ilmenite ore (IL) were collected from Abu Ghalaga area, and then a facile chemical functionalization is applied to produce functionalized ilmenite (f-IL). The detoxification of Pb(II) ions was carried out in this study by photocatalytic method in an aqueous solution. In this approach, Pb(II) adsorption by $FeTiO_3$ is characterized by its large surface area, excellent stability and low cost.

2. Experimental

In this study, natural ilmenite ores were procured from the Abu Ghalaga area, in Egypt. Hydrogen peroxide (H_2O_2, 30 wt%) was purchased from El Nasr Pharmaceutical Chemicals Company, and $Pb(CH_3COO)_2$ was purchased from Sigma Aldrich company. All received materials were used without further purification.

Geologic setting

Abu Ghalaga area lies about 25 km southwest of Abu Ghusun City on the Red Sea Coast and far about 125 km from Marsa Alam city. Abu Ghalaga area is considered the largest ilmenite reserve ore in Egypt. The Neoproterozoic rocks of the Wadi Abu Ghalaga area include island-arc metavolcanics, intrusive layered gabbro and syn-tectonic granitoids [22] (**Fig. 1**). These rock units are dissected by several dykes of various compositions. In addition, many quartz veins crosscut the country rocks of the study area. The metavolcanics are the oldest rock units exposed in Wadi Abu Ghalaga area. They represent mainly by mafic metavolcanics (metabasalt) and felsic metavolcanics (metadacite and metarhyolite) with their pyroclastics (**Fig 2**).

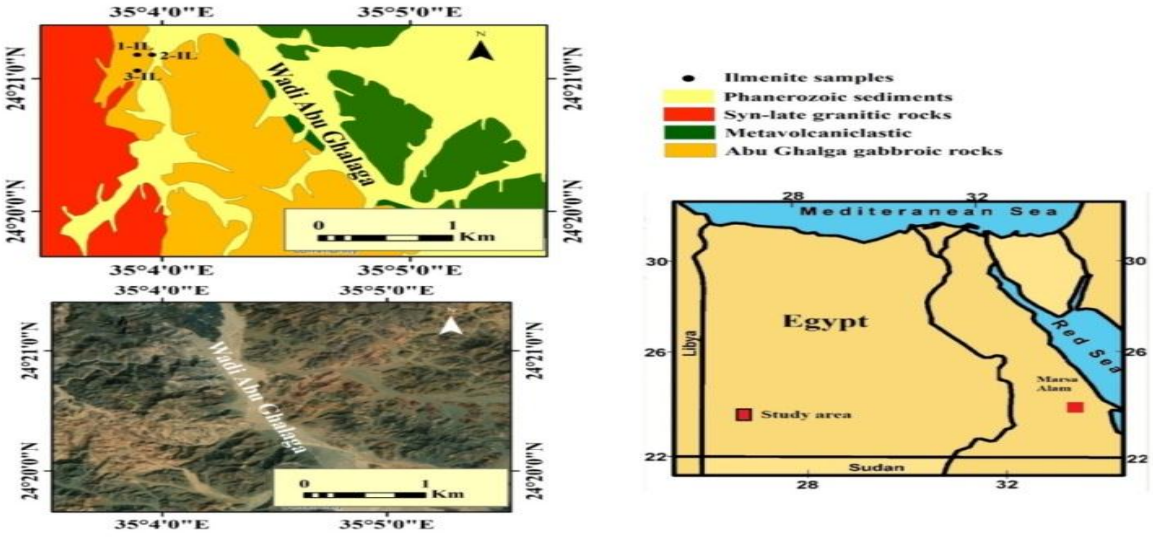

Fig 1. Geologic map Wadi Abu Ghalaga area [22].

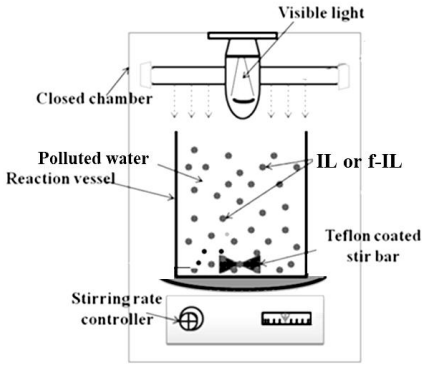

Fig 3. Photoreactor for Pb(II) photocatalytic removal processes.

Fig 2. Sheet of fresh ilmenite with sharp contact against gabbro.

Synthesis of hydroxyl-functionalized ilmenite samples

The –OH functionalization method was carried out with few modifications according to pervious work conducted by Dhineshbabu group [23]. Briefly, about 1 g of natural ilmenite samples (with serial number **1-IL**, **2-IL**, and **3-IL** based on their ore source location) were sonicated in 100 mL of H_2O_2 for 15 min, followed by refluxing at boiling temperature for 4 h. The resulting solution was filtered, washed several times, and dried at 80 ˚C in oven.

Characterization of ilmenite ores and chemically functionalized ilmenite

X-ray Fluorescence (XRF) analysis

XRF analyses were performed at the GeoAnalytical Lab, USA. The concentration of the major was determined by X-ray fluorescence (ThermoARL XRF Spectrometer). Each sample was weighed, mixed with two parts di-lithium tetraborate flux, fused in a muffle furnace at 1000°C, and then cooled. The resulting bead was reground, re-fused, and polished on the diamond lap producing a smooth, flat surface for analysis. The calibration standard was the reference material 650CC from the USGS standard rock powder GSP2. The loss on ignition (LOI) was determined by the weight difference after ignition at 1000 °C. A working curve for instrument sensitivity was developed using a blank fused bead from the same batch of flux as used to prepare the unknowns along with USGS standards AGV-2 and RGM-2. To control for quality, additional USGS standards (DTS-2, BCR-1, G-2) were included as unknowns.

X-Ray Diffraction (XRD) analysis

Minerals identification of three samples of ilmenite ores of Abu Ghalaga were achieved by XRD at the Egyptian Mineral Resources Authority (Dokki, Egypt). XRD analyses were detected using a PANalytical X-ray diffraction equipment model X′Pert PRO with a Secondary Monochromator. Cu-radiation (λ=1.542Å) at 45 K.V., 35 M.A.

Scanning Electron Microscope (SEM) analysis

The surface morphology and chemical composition analysis were performed using SEM, FEI Quanta FEG-250 microscope, equipped with AMETEK unit, is the energy dispersive X-ray spectroscopy (EDX) analysis unit, with an accelerating voltage of 20 kV. The samples were prepared by mounting them on an aluminum holder by carbon adhesive tape prior to scanning.

Fourier Transmission Infrared (FTIR) analysis

The FTIR spectra were recorded using Bruker VERTEX-80v vacuum FTIR spectrometer from 4000 to 400 cm^{-1}.

Nitrogen adsorption-desorption analysis

Table 1. Major oxides by XRF of ilmenite ore of Abu Ghalaga area.

Samples	1-IL	2-IL	3-IL
Major and minor oxides	Abundant %		
SiO_2	2.75	0.57	1.91
TiO_2	36.61	39.53	39.73
Al_2O_3	0.94	0.04	0.29
Fe_2O_3	55.15	57.50	55.04
MgO	3.26	1.82	2.39
CaO	0.25	0.25	0.01
Na_2O	<d.l.	<d.l.	<d.l.
K_2O	0.03	<d.l.	<d.l.
P_2O_5	0.02	0.02	0.01
MnO	0.21	0.24	0.21
LOI	1.29	0.28	1.24
Total	100.52	100.25	100.83

The specific surface area and porous structure were characterized by the nitrogen adsorption-desorption measurements at liquid N_2 temperature (77K). The data were collected by NOVA Touch LX4, Quantachrome instruments. All ilmenite samples were degassed at 250˚C for 3 h prior to measurements.

Application of ilmenite samples (before and after functionalization) for removal of Pb(II) ions.

Photocatalytic removal of Pb(II) ions was studied using a mixture solution containing 20 mL of Pb(II) ions (50 ppm) and 0.02 g of f-IL composites (**1-IL**, **1-f-IL**, **2-IL**, **2-f-IL**, **3-IL**, **3-f-IL**) in an Erlenmeyer flask.

Then, the glass apparatus was placed in a photoreactor (**Fig 3**) equipped with magnetic stirrer (200 rpm stirring rate) for 60 min under visible light irradiation using four LED lamps Philips 20 watt as source of visible light. Afterward, the mixture was centrifuged at 3000 rpm for 5 minutes. The filtrate was taken out and measured by Atomic Absorption Spectrometer (Varian SpectrAA 220).

The removal efficiency was calculated according to the following equation:

$$R\% = [(C_0-C_1)/C_0] \times 100$$, where:

R%: Removal efficiency, C_0: initial concentration of metal ions before treatment, C_1: the concentration of metal ions after treatment.

3. Results and discussion

Characterization of ilmenite samples as $FeTiO_3$ photocatalyst (before and after functionalization)

XRF Analysis

XRF data for three collected samples from Abu Ghalaga ilmenite ores were determined (Table 1).

The XRF data of bulk chemical analyses are listed in (**Error! Reference source not found.**) TiO_2 (36.61-39.73 wt%) and Fe_2O_3 (55.04-55.15 wt%) represent the major oxides in the analyzed ilmenite samples with minor amounts of SiO_2 (0.57-2.75 wt%) and MgO (1.82-3.26 wt%). Other major oxides are very low in their concentrations or below the detection limits. The analyzed ilmenite samples have low LOI values (0.18-1.58 wt%) indicating the fresh nature of these samples.

XRD Analysis

The main mineral in the Abu Ghalaga ilmenite ore samples is ilmenite Fe (TiO_3) ranging from (80%) for sample (**1-IL**) and (83%) for sample (**2-IL**) and (78%) for sample (**3-IL**). While the hematite mineral (Fe_2O_3) ranging from (20%) for sample (**1-IL**), (17%) for sample (**2-IL**), and (22%) for sample (**3-IL**) (Error! Reference source not found. **and Table 2**).

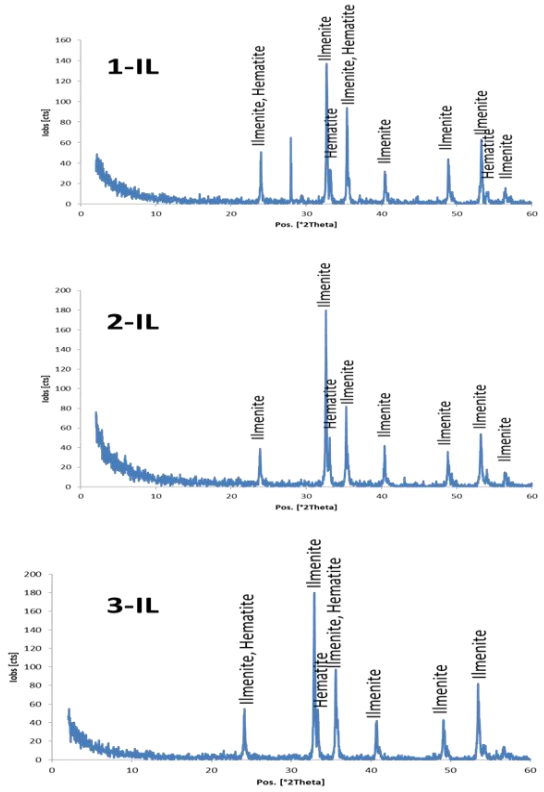

Fig.4. XRD pattern of ileminte ore samples

Table 1. Major oxides by XRF of ilmenite ore of Abu Ghalaga area.

Samples	1-IL	2-IL	3-IL
Major and minor oxides	**Abundant %**		
SiO_2	2.75	0.57	1.91
TiO_2	36.61	39.53	39.73
Al_2O_3	0.94	0.04	0.29
Fe_2O_3	55.15	57.50	55.04
MgO	3.26	1.82	2.39
CaO	0.25	0.25	0.01
Na_2O	<d.l.	<d.l.	<d.l.
K_2O	0.03	<d.l.	<d.l.
P_2O_5	0.02	0.02	0.01
MnO	0.21	0.24	0.21
LOI	1.29	0.28	1.24
Total	100.52	100.25	100.83

Table 2. XRD of ilmenite ore of Abu Ghalaga area.

Sample	1-IL	2-IL	3-IL
Composition of ore	**Abundant %**		
Ilmenite Fe(TiO_3)	80	83	78
Hematite Fe_2O_3	20	17	22

FTIR analysis

Fourier Transform Infrared (FTIR) analysis was used to investigate the binding structure of ilmenite before and after the H_2O_2 functionalization process as presented in

Fig . From the FTIR spectra, all samples show bands around 450, 530, and 685 cm^{-1}, which correspond to the characteristic vibration bands of ilmenite, as reported in previous studies [24, 25]. The bands appeared between 500-1000 cm^{-1} are attributed to Ti-O-Ti and Fe-O vibrational modes [26, 27]. Sharpened and more intensive bands exhibited in **1-f-IL** and **3-f-IL** samples, with shift in peak positions, indicating the increase in material crystallinity after treatment and confirming the interaction between ilmenite and H_2O_2. On contrarily, sample **2-f-IL** exhibited broader and less intensive bands in comparison to untreated **2-IL** sample, due to presence of impurities and difference in ilmenite ore composition as reported by the XRF analysis. Furthermore, a broad weak band is clearly observed at 1632.92 cm^{-1} for the functionalized sample **1-f-IL**, which is assigned to -OH bending vibration [28]. A study done by Wijewardhana group mentioned that the band at 1630 cm^{-1} is assigned to Ti-OH vibrations [27]. All the untreated ilmenite samples displayed various bands from 2600 to 3600 cm^{-1} that denote to the -OH

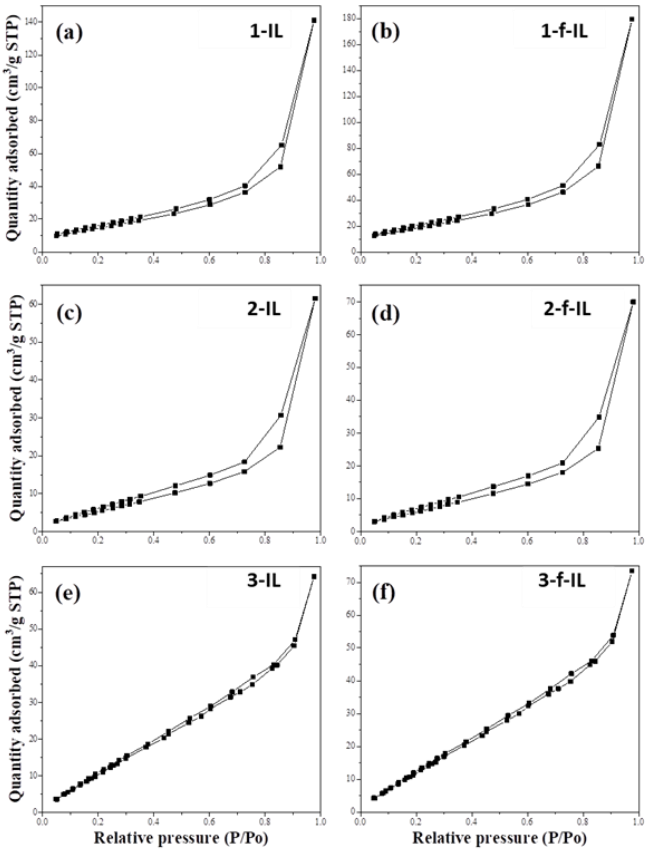

stretching vibrations of adsorbed water molecules [29, 30]. However, some of these bands became smaller or disappeared after treatment with H_2O_2 that is attributed to the thermal treatment conducted after functionalization process [31].

Nitrogen adsorption-desorption analysis

The Braunauer-Emmett-Teller (BET) method was employed to calculate the specific surface area (SSA).

The pore volume and size distributions were obtained from the nitrogen adsorption-desorption isotherms.

From the results listed in Error! Reference source not found., the functionalized ilmenite samples displayed higher SSA and total pore volume in comparison to untreated ones. The SSA for ilmenite samples **1-IL**, **2-IL**, **3-IL**, **1-f-IL**, **2-f-IL**, and **3-f-IL** are 56.032, 24.7546, 62.0669, 71.3135, 28.1302, and 70.9337 m^2/g respectively. These results are superior in comparison to that listed in the literature, where the natural ilmenite ore (both treated and untreated) exhibited low SSA varied from 0.15 to 13.20 m^2/g [32–36].

While the synthetic nano-$FeTiO_3$ ranged from 40.77 to 115 m^2/g [30,37] .

Table 3. The specific surface area, pore sizes, and pore volume distribution for all ilmenite samples.

Adsorbent	SSA (m^2/g)	Total pore (cm^3/g)	Average pore size (nm)
1-IL	56.032	0.218614	7.80319
2-IL	24.7546	0.0954811	7.71421
3-IL	62.0669	0.0996729	3.21179
1-f-IL*	71.3135	0.278236	7.80319
2-f-IL	28.1302	0.108501	7.71421
3-f-IL	70.9337	0.113912	3.21179
* **1-f-IL** displayed the highest surface area, pore volume, and pore size.			

After functionalization, the ilmenite samples showed larger total pore volume values ranged from 0.109 cm^3/g to 0.278 cm^3/g, indicating a higher adsorption capacity for heavy metals. On contrarily, the average pore sizes were not affected by functionalization and varied from 3.2 to 7.8 nm, which belong to the mesoporous materials according to the IUPAC classification [38]. From the adsorption-desorption isotherms presented in Error! Reference source not found., all curves are characteristic to Type (III) isotherm.

It was obvious that, sample **1-f-IL** exhibited the highest SSA, total pore volume, and average pore size, suggesting it will be a more effective adsorbent than other ilmenite samples towards adsorption of heavy metals in wastewater. These findings corroborate with the observations acquired from the SEM images.

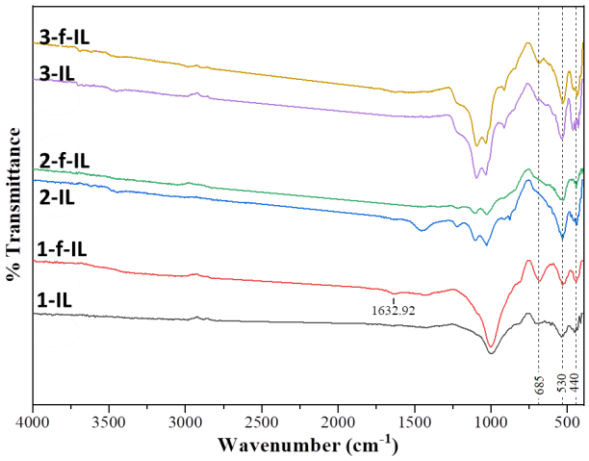

Fig 5. The FTIR spectra for the ilmenite samples before and after functionalization.

Fig 6. The adsorption-desorption isotherms for all the ilmenite samples.

SEM analysis

Error! Reference source not found. displays the surface morphology of the ilmenite samples before and after functionalization **1-IL**, **3-IL**, **1-f-IL**, **3-f-IL**; respectively that showed higher surface area, pore volume, and pore size. Sample **1-IL** reveals macro-shaped lumps with few ununiformed small particles. While, small and large uneven particles with minor lamellar shapes are visible in the **1f-IL** sample, indicating a significant increase in surface area.

Beside the irregular shaped lumps and particles, sample **3-IL** shows macro lamellar shapes with a size range of 0.2-1.4 µm, which decreased to 0.06-1.0 µm with a flaky-like surface morphology for the treated **3-f-IL** sample confirming the increase in surface area **Fig 7.** The SEM and EDX micrographs at different magnifications for the 1-**IL**, **1-f-IL**, **3-IL**, and **3-f-IL** ilmenite samples.

Application of ilmenite samples on adsorption of Pb(II) ions in a synthetic solution

Effect of contact time

In this work, the ilmenite composites (**1-IL**, **1-f-IL**, **2-IL**, **2-f-IL**, **3-IL**, **3-f-IL**) were tested to adsorb Pb(II) ions as one of the major pollutants of water. The experiments were performed in ambient and under the effect of visible light by adding 5 mg to the

after functionalization. The ilmenite ores' heterogeneous, porous and irregular structure is clearly visible in all micrographs, with apparent difference in surface roughness between the treated and untreated samples.

The quantitative energy dispersive X-ray spectroscopy (EDX) analysis displays the elemental composition of ilmenite samples, which is primarily composed of Ti, Fe, and O with minor amounts of C, Mg, Si, Na, Al, P, S, and Ca. These results are consistent with the chemical composition obtained by the XRF analysis. The apparent variation in the surface topology between untreated ilmenite samples was related to its ore source.

synthetic solution of the lead acetate [initial concentration (C_0) of copper solution equals to 50 ppm] at pH 7.

Table 4. Effect of contact time on Pb(II) ions removal in: (a) Ambient condition and (b) under visible light irradiation condition.

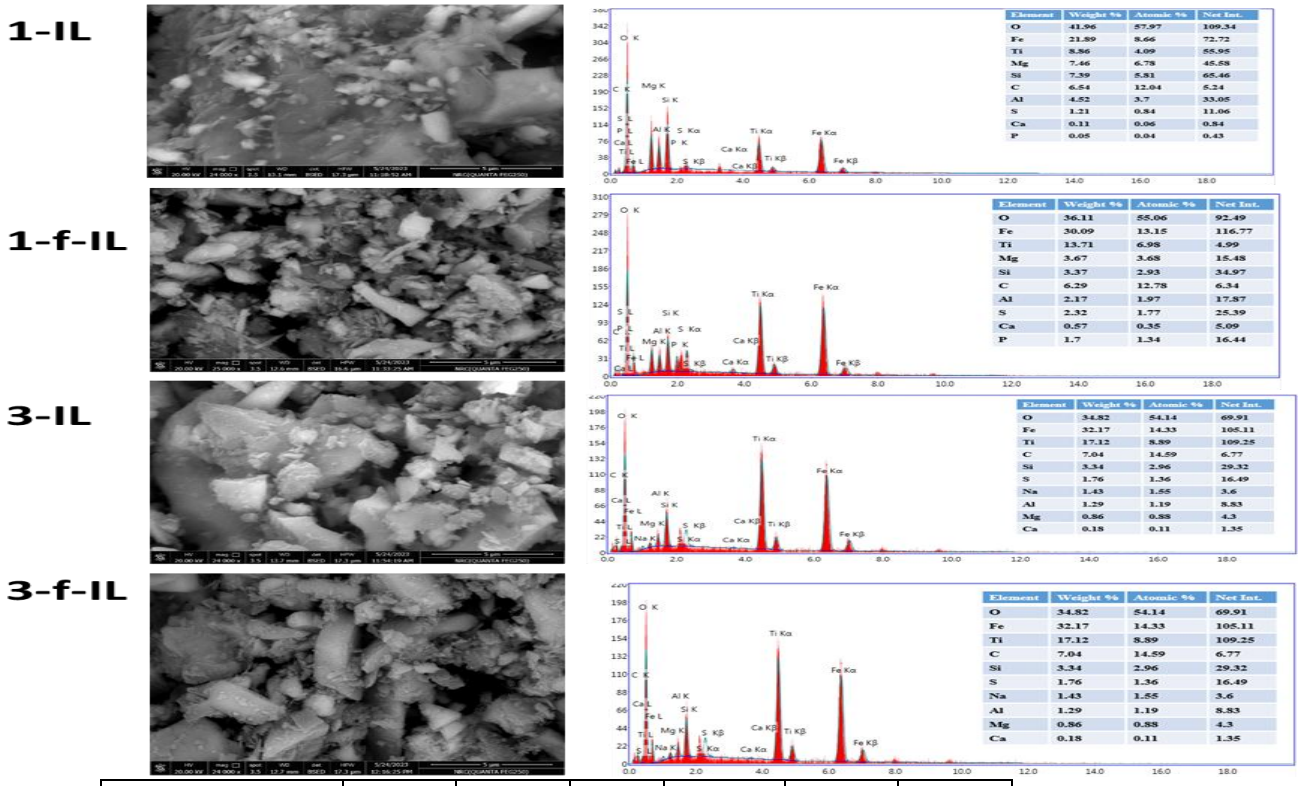

Sample	1-IL	1-f-IL	2-IL	2-f-IL	3-IL	3-f-IL

Contact time (min)		Removal efficiency of Pb(II) ions %					
(a) Ambient condition	**5**	36.3	42.8	3.1	6.7	21.2	27.6
	10	36.9	43.1	3.5	7.9	21.3	27.8
	15	37.1	43.7	5.6	8.2	22.7	28.3
	20	38.2	44.6	6.2	8.7	23.3	29.1
	25	39.6	44.7	6.8	9.4	24.6	30.7
	30	40.1	45.1	7	10.3	24.6	31.9
	40	40.7	45.2	7.1	10.2	24.6	31.1
	50	40.7	45.2	7.1	10.2	24.6	31.1
	60	40.7	45.2	7.1	10.2	24.6	31.3
(b) Visible light irradiation condition	**5**	56.3	56.3	7.6	11.7	33.2	41.6
	10	58.1	57.1	7.8	17.2	34.6	43.8
	15	59.9	60.2	10.2	19.4	35.5	44.2
	20	60.5	62.4	11.4	21.9	37.1	44.6
	25	61.8	63.2	11.9	22.1	37.7	44.9
	30	62.3	67.5	12.1	22.3	38.3	45.7
	40	62.6	67.5	12.3	22.3	38.3	45.7
	50	62.5	67.6	12.4	22.3	38.3	45.7
	60	62.5	67.6	12.4	22.3	38.3	45.7

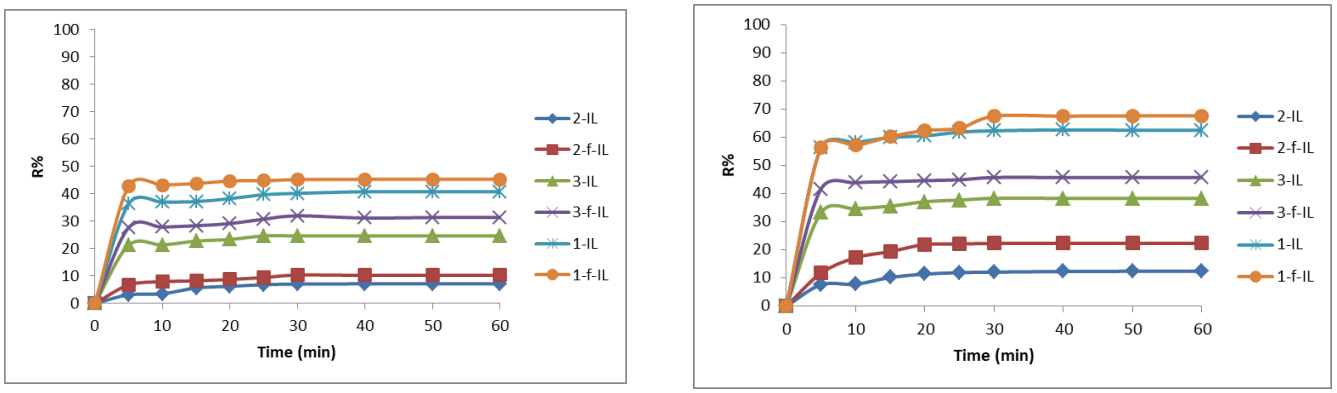

Fig 8. Effect of contact time on Pb(II) ions removal: (a) in dark and (b) under visible light irradiation conditions.

From the results presented in Figure 8 and Table 4, it is noticeably that the light has an improvement role in increasing the absorptivity of lead. The samples **2-IL** and **2-f-IL** showed the lowest activity under both dark and visible irradiation. However, **1-f-IL** composite displayed the highest removal efficiency reaching 67.6% after 60 min under visible light irradiation.

The samples **2-IL** and **2-f-IL** showed the lowest activity under both dark and visible irradiation.

However, **1-f-IL** composite displayed the highest removal efficiency reaching 67.6% after 60 min under visible light irradiation.

Effect of adsorbent loading

The experiments were performed under the effect of ambient conditions at pH 7 and 25 ^{o}C using different amounts (5 mg, 10 mg, 15 mg, 20 mg) of the samples; **1-IL**, **1-f-IL**, **2-IL**, **2-f-IL**, **3-IL** and **3-f-IL** were used to reach the maximum adsorption for Pb^{2+} ions after 60 min under visible light irradiation.

Figure 9 showed that samples **2-IL** and **2-f-IL** exhibited weak adsorption effect. However, a significant increase in the removal efficiency had been observed when the titanium oxide ratio increased in the samples **1-IL** and **3-IL**. Additionally, the functionalized ilmenite samples **1-f-IL** and **3-f-IL** showed improved Pb^{2+} adsorption. It was obvious that **1-f-IL** exhibited the best performance for removal of Pb^{2+} ions with 97.6% removal efficiency at 20 mg of the sample; all other results were listed in **Table 5**.

Effect of pH

The effect of pH on photocatalytic removal of Pb(II) ions has been investigated. As illustrated in **Figure 10** and **Table 6**, it is obviously observed that the removal efficiency (R%) starts to increase till

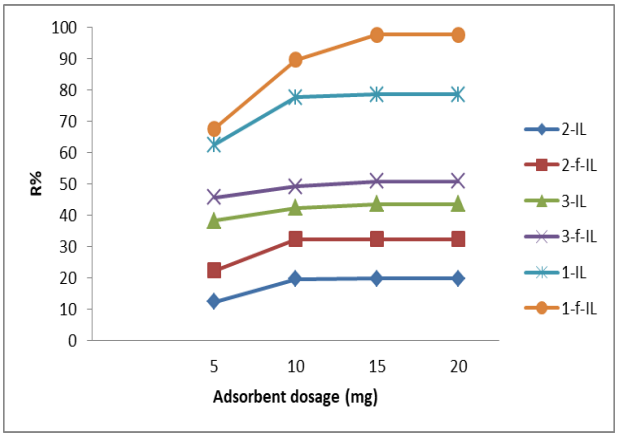

Fig. 9. Effect of adsorbent loading in removal of Pb(II) ions.

Table 5. Effect of adsorbent dosage on Pb(II) ions removal.

Adsorbent dosage (mg)	**5**	**10**	**15**	**20**
Samples	Removal efficiency of Pb(II) ions %			
1-IL	62.5	77.5	78.5	78.5
1-f-IL	67.6	89.6	97.6	97.6
2-IL	12.4	19.7	19.8	19.8
2-f-IL	22.3	32.3	32.3	32.3
3-IL	38.3	42.3	43.6	43.6
3-f-IL	45.7	49.2	50.8	50.8

reaching its maximum at pH 7 then decrease with increasing pH to 9. It was confirmed that after pH 7, the Pb(II) began to precipitate, and Pb(II) in the solution form was unstable. This is attributed to the precipitation of Pb(II) species in the form of $Pb(OH)_2$ at pH 9. Besides, the surface of $FeTiO_3$ can be converted to $FeTiO^-$, which is not easy to release electrons under light irradiation conditions. Therefore, these findings confirm the great influence of solution pH on the photocatalytic removal of Pb(II) ions and the optimum conditions was achieved at pH 7, temperature 25 ^oC, and catalyst dosage 20 mg under visible light conditions. In addition to the superior photocatalytic removal efficiency of the functionalized samples compared to their natural ores under optimum conditions. The best removal efficiency is achieved for sample **1-f-IL** reaching 97.6% and the lowest performance is observed for sample **2-IL** with 19.8% removal efficiency.

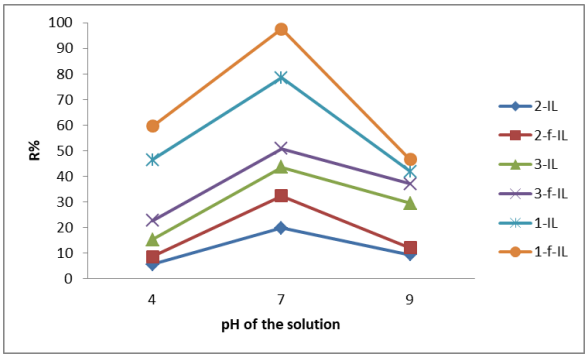

Fig 4. Effect of pH of the solution ranging from 4-9 on photocatalytic removal of Pb(II) ions under visible light irradiation, 25 ^oC, f-IL conc. 20 mg.

Adsorption isotherm

The removal of Pb(II) without irradiation of light indicated that adsorption of Pb(II) occurred on the Fe_3O_4 surface that act as a host material. The maximum adsorption capacity of Pb(II) on **f-IL** composite **1-f-IL** can be determined using the Langmuir isotherm model.

$$\frac{Ce}{qe} = \frac{Ce}{qm} + \frac{1}{KL\,qm}$$

Ce is the concentration of Pb(II) solution (mg/L), qe is the quantity of Pb(II) adsorbed per 1 g of catalyst (mg/g), qm is the maximum adsorption capacity (mg/g), and KL is the Langmuir adsorption constants that is related to the adsorption energy (L/mg). Based on the adsorption isotherm graph (Error! Reference source not found.), the maximum adsorption capacity (qm) value and the Langmuir adsorption constant (KL) of the nanocomposite to Pb(II) molecules were calculated from the equation of the line curve qe versus Ce (Error! Reference source not found.).

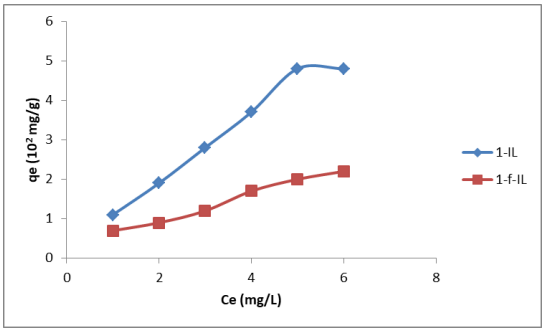

Fig. 11. Effect of adsorbent loading in removal of Pb(II) ions.

Table 7. The Langmuir isotherm constant and kinetics for photocatalytic removal of Pb(II) ions.

Sample	qm (10^2 mg / g)	KL (10^{-1} L / mg)	R^2 (%)
1-f-IL	309.7	0.0991	0.98
1-IL	124.5	0.0465	0.97

Mechanism insight

The adsorption of Pb(II) on nanocomposite followed the Langmuir isotherm model proposed that the highest adsorption capacity of Pb(II) was induced on the surface of sample **1-IL** and **1-f-IL** with $FeTiO_3$ comprising of (TiO_2 36.61%, Fe_2O_3 55.15%) in presence of metal oxides accompanied with the ore (SiO_2, Al_2O_3, MgO; 2.75%, 0.94%, 3.26%) (XRF data, **Table 1**). Although the highest TiO_2 content was observed in samples **2-IL** and **3-IL**; 39.53% and 39.73% respectively, the sample **1-f-IL** showed the most effective adsorbent. That could refer to the accompanied metal oxide in the ore **1-IL** or **1-f-IL**. It can be postulated that the hydroxyl groups on metal oxide in water are acting as sites for ion exchange [39] With this phenomenon, it is hypothesized that chelate complexes between $FeTiO_3$ and Pb^{2+} ions were formed to form $[FeTiO_3]$-[Pb] (**Complex-I**) $[FeTiO_3$-(OH)x]-[Pb] or (**Complex-II**) in both cases before and after functionalization with hydroxyl group (**Fig. 12**). From the isotherm results (Table 7), it was worth noting that the adsorption of Pb(II) ions removal needed more active hydroxyl groups on $FeTiO_3$ surface that was achieved after functionalization of sample **1-IL** with hydroxyl groups to produce sample **1-f-IL**. As a result, it was observed that the **1-f-IL** sample exhibited the maximum adsorption capacity value (qm = 309.7 mg/g). In addition, from the experiments, it was determined that that performing the adsorption process under visible light irradiation, an enhancement in the adsorption ability of Pb^{2+} over **f-IL** adsorbents was observed. The highest removal efficiency was recorded for **1-f-IL** sample 97.6% under optimized conditions. The photocatalytic removal for Pb^{2+} ions can be expressed by the following equations.

$FeTiO_3$ or $FeTiO_3$-OHx + hv → $[FeTiO_3]$* or $[FeTiO_3$-OHx]* + e^- + h^+ (Sensitization)
$H_2O \rightarrow HO^- + H^+$ (Water splitting)
$Pb^{2+} + {}^{\cdot}OH \rightarrow PbO + H^+$ (Photo-oxidation)

As a result, it can be concluded that the removal of Pb^{2+} under light conditions can be accomplished through photo-oxidation approach [12].

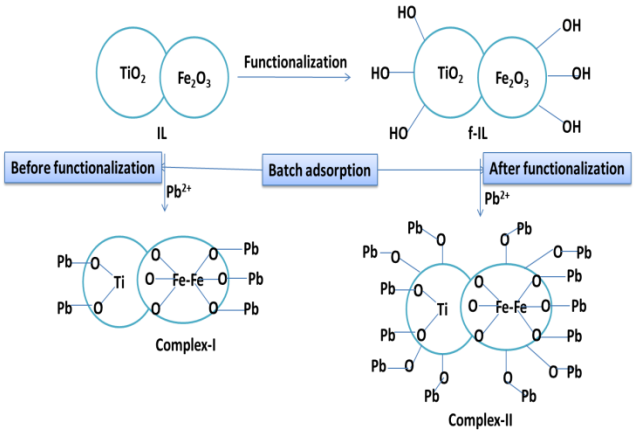

Fig 12. Postulated batch adsorption of Pb^{2+} on IL or f-IL adsorbents

Conclusion

In this study, the Egyptian Abu Ghalaga natural ilmenite ores (**IL**) were successfully functionalized with hydrogen peroxide through a simple method. The formation of hydroxyl functional group after functionalization was attributed to the surface modification process of ilmenite, where (-OH) functional groups are introduced on the ilmenite surface besides its increased surface area and pore volume, that improves its photocatalytic performance and promotes adsorption of Pb(II) ions. As a result, it was observed that, the Pb(II) ions were efficiently removed from aqueous solution under visible light irradiation after 60 min irradiation time at pH 7, room temperature, and catalyst dosage 20 mg. It was determined that the sample **1-f-IL** recorded the highest removal efficiency 97.6% and maximum adsorption capacity [i.e. maximum adsorption of Pb^{2+} ions per 1g of catalyst (mg/g)] 309.7 mg/g, respectively. Thus, these findings are promising for developing new, green, non-toxic, low-cost, and effective photocatalytic materials for water treatment applications.

Abbreviations:

XRF: X-ray Fluorescence
XRD: X-ray Differaction
SEM: Scan Electron Microscope
EDX: Energy Dispersive X-ray
FTIR: Fourier Transform Infrared
BET: The Braunauer-Emmett-Teller

Conflict of interests

The authors declare there is no conflict of interest.

Compliance with ethical standards

The authors have declared no conflict of interest.

Ethical approval
This type of study formal consent is not required.
Statement on the welfare of animals
This report does not contain any studies with human participants or animals performed by any of the authors.

Authorship responsibility and contribution
Yasser M. A. Mohamed (y.m.a.mohamed@outlook.com): Corresponding author. Designed the experiments, participated in the sequence, alignment of the manuscript, analysis the data and sharing in writing the manuscript.
Ahmed A. Elnazer (nazer42@yahoo.com): Corresponding author. Identification of minerals, participated in the sequence, analysis the data and sharing in writing the manuscript.
Mokhles A. Azer (mokhles72@yahoo.com): Analysis the data, participated in the sequence, alignment of the manuscript and sharing in writing the manuscript.
Elzahraa, A. Elgohary (chemistzahra2000@gmail.com): Analysis the data and participated in the experiments, alignment of the manuscript and sharing in writing the manuscript.
Hossam A. El Nazer (dr_hosamnazer@yahoo.com): Analysis the data, participated in the sequence, alignment of the manuscript and sharing in writing the manuscript.

Consent to participate
We, (the authors) hereby declare that we participated in this study and development of this article.

Consent to publish
We, the authors have read final version of this article and give our consent to be published.

Availability of data and materials
The authors confirm that the data supporting the findings of this study are available within the article.

Acknowledgment
The authors acknowledge National Research Center (Egypt) for their valuable support through research project fund (Project title: "Production of cheap photoactive nano-hybrids from natural resources for water treatment", ID: 13020204).

References
[1] Bahadir, T., Şimşek, İ., Tulun, Ş., & Çelebi, H. Use of different food wastes as green biosorbent: Isotherm, kinetic, and thermodynamic studies of Pb2+. Environmental Science and Pollution Research. (2023). https://doi.org/10.1007/s11356-023-29745-6
[2] Awual, Md. R., Hasan, Md. M., Iqbal, J., Islam, A., Islam, Md. A., Asiri, A. M., & Rahman, M. M. Naked-eye lead(II) capturing from contaminated water using innovative large-pore facial composite materials. Microchemical Journal, 154, 104585. (2020). https://doi.org/10.1016/j.microc.2019.104585
[3] Awual, Md. R.. An efficient composite material for selective lead(II) monitoring and removal from wastewater. Journal of Environmental Chemical Engineering, 7(3), 103087. (2019). https://doi.org/10.1016/j.jece.2019.103087
[4] Wang, C., Wang, X., Li, N., Tao, J., Yan, B., Cui, X., & Chen, G.. Adsorption of Lead from Aqueous Solution by Biochar: A Review. Clean Technologies, 4(3), 629–652. (2022). https://doi.org/10.3390/cleantechnol4030039
[5] Wu, J., Wang, T., Wang, J., Zhang, Y., & Pan, W.-P. A novel modified method for the efficient removal of Pb and Cd from wastewater by biochar: Enhanced the ion exchange and precipitation capacity. Science of The Total Environment, 754, 142150. (2021). https://doi.org/10.1016/j.scitotenv.2020.142150
[6] Jadoun, S., Fuentes, J. P., Urbano, B. F., & Yáñez, J. A review on adsorption of heavy metals from wastewater using conducting polymer-based materials. Journal of Environmental Chemical Engineering, 11(1), 109226. (2023) https://doi.org/10.1016/j.jece.2022.109226
[7] Abd El-Aziz, M. E., Morsi, S. M. M., Kamal, K. H., Khattab, T. A. Preparation of Isopropyl Acrylamide Grafted Chitosan and Carbon Bionanocomposites for Adsorption of Lead Ion and Methylene Blue. Polymers, 14(21), 4485; (2022). https://doi.org/10.3390/polym14214485
[8] Fayez, A., Kamel, A. H., Hassan, A. S. M., Abd El-Aziz, M. E., Youssef. A. M. Development and utilization of Chitosan/Carbon Nanocomposite for heavy metal removal from wastewater. The Egyptian Journal of Chemistry. 65(9) 559-569, (2022).
[9] Mohamed, Y.M.A., Abd El-Aziz, M. E., Kamal, K. H., Elgohary, E. A., Stafford, J., Davies, P., El Nazer, H. A. Employment and performance of modified chitosan for the removal of copper ions and methylene blue in wastewater. Polymer Engineering and Science, 63(6) 1836-1850, (2023). https://doi.org/10.1002/pen.26329
[10] Abd El-Aziz, M. E., Youssef. A. M, Kamal, K. H., Kelnar, I., Kamel, S. Preparation and performance of bionanocomposites based on grafted chitosan, GO and TiO2-NPs for removal of lead ions and basic-red 46 Carbohydrate Polymers
305, 120571, (2023)
[11] Zhao, X., Jia, Q., Song, N., Zhou, W., & Li, Y. Adsorption of Pb(II) from an Aqueous Solution by Titanium Dioxide/Carbon Nanotube Nanocomposites: Kinetics, Thermodynamics, and Isotherms†. Journal of Chemical & Enineering

Data, 55(10), 4428–4433. (2010). https://doi.org/10.1021/je100586r

[12] Mostafa, N. G., Yunnus, A. F., & Elawwad, A. Adsorption of Pb(II) from Water onto ZnO, TiO2, and Al2O3: Process Study, Adsorption Behaviour, and Thermodynamics. Adsorption Science & Technology, Article,ID,7582756,(2022). https://doi.org/10.1155/2022/7582756

[13] Rehman, M., Rehman, W., Waseem, M., Hussain, S., Haq, S., & Rehman, M. A. Adsorption mechanism of Pb2+ ions by Fe3O4, SnO2, and TiO2 nanoparticles. Environmental Science and Pollution Research, 26(19), 19968–19981, (2019). https://doi.org/10.1007/s11356-019-05276-x

[14] Elgohary, E. A., Mohamed, Y. M. A., El Nazer, H. A., Baaloudj, O., Alyami, M. S. S., El Jery, A., Assadi, A. A., & Amrane, A. A Review of the Use of Semiconductors as Catalysts in the Photocatalytic Inactivation of Microorganisms. Catalysts, 11(12), (2021). https://doi.org/10.3390/catal11121498

[15] Elgohary, E. A., Mohamed, Y. M. A., Rabie, S. T., Salih, S. A., Fekry, A. M., & El Nazer, H. A. Highly selective visible-light-triggered CO2 fixation to cyclic carbonates under mild conditions using TiO2/multiwall carbon nanotubes (MWCNT) grafted with Pt or Pd nanoparticles. New J. Chem., 45(37), 17301–17312,(2021). https://doi.org/10.1039/D1NJ03123F

[16] Wahyuni, E. T., Rahmaniati, T., Hafidzah, A. R., Suherman, S., & Suratman, A. Photocatalysis over N-Doped TiO2 Driven by Visible Light for Pb(II) Removal from Aqueous Media. Catalysts, 11(8), 945, (2021). https://doi.org/10.3390/catal11080945

[17] Obiri, S., Gobinah, R., Essumang, D. K., Armah, F. A., Ason, B., Tagbor, T. A., & Kirgiz, S. M. Extraction of TiO2 from kaolin deposits in the Central Region, Ghana: An alternative material for the formulation of climate-smart Portland cement. Materials Today: Proceedings, 66(Part 4), 2559–2567, (2022). https://doi.org/10.1016/j.matpr.2022.07.090

[18] Thambiliyagodage, C., Mirihana, S., Wijesekera, R., Madusanka, D. S., Kandanapitiye, M., & Bakker, M. Fabrication of Fe2TiO5/TiO2 binary nanocomposite from natural ilmenite and their photocatalytic activity under solar energy. Current Research in Green and Sustainable Chemistry, 4, 100156,(2021). https://doi.org/10.1016/j.crgsc.2021.100156

[19] Van Gosen, B. S., & Ellefsen, K. J. Titanium mineral resources in heavy-mineral sands in the Atlantic coastal plain of the southeastern United States (Report 2018–5045; Scientific Investigations Report, p. 32). USGS Publications Warehouse, (2018). https://doi.org/10.3133/sir20185045

[20] Ali, R. A. M., Mobarak, M., Badawy, A. M., Lima, E. C., Seliem, M. K., & Ramadan, H. S. New insights into the surface oxidation role in enhancing Congo red dye uptake by Egyptian ilmenite ore: Experiments and physicochemical interpretations. Surfaces and Interfaces, 26, 101316, (2021). https://doi.org/10.1016/j.surfin.2021.101316

[21] Khedr MZ, Takazawa, E., Arai,S., Stern, R. G., Morishita, T., El-Awady, A. Styles of Fe–Ti–V ore deposits in the Neoproterozoic layered mafic-ultramafic intrusions, south Eastern Desert of Egypt: Evidence for fractional crystallization of V-rich melts, Journal of African Earth Sciences, 194. (2022)

[22] Abdelsalam, E. M., Mohamed, Y. M. A., Abdelkhalik, S., El Nazer, H. A., & Attia, Y. A. Photocatalytic oxidation of nitrogen oxides (NOx) using Ag- and Pt-doped TiO2 nanoparticles under visible light irradiation. Environmental Science and Pollution Research, 27(28), 35828–35836, (2020). https://doi.org/10.1007/s11356-020-09649-5

[23] Mohamed, Y. M. A., & Attia, Y. A. Nano Pt/TiO2 photocatalyst for ultrafast production of sulfamic acid derivatives using 4-nitroacetanilides as nitrogen precursor in continuous flow reactors. Environmental Science and Pollution Research, (2023). https://doi.org/10.1007/s11356-023-25968-9

[24] Mohamed, Y. M. A., Elgohary, E. A., Rabie, S. T., Salih, S. A., Fekry, A. M., & El Nazer, H. A. Palladium-Modified TiO2/MWCNTs for Efficient Carbon Capture and Photocatalytic Reduction of Nitro-aromatic Derivatives. ChemistrySelect, 8(5), e202203098,(2023). https://doi.org/10.1002/slct.202203098

[25] Abdelhafiz, M. A., Seleem, E.-M. M., El Nazer, H. A., Zeid, S. A. M., Salman, S. A., & Meng, B. Shallow groundwater environmental investigation at northeastern Cairo, Egypt: Quality and photo-treatment evaluation. Environmental Geochemistry and Health, 43(11), 4533–4551, (2021). https://doi.org/10.1007/s10653-021-00933-y

[26] Saleh, G. M., Khaleal, F. M., & Lasheen, E. S. R. Petrogenesis of ilmenite-bearing mafic intrusions: A case study of Abu Ghalaga area, South Eastern Desert, Egypt. Arabian Journal of

Geosciences, 15(18), 1508, (2022). https://doi.org/10.1007/s12517-022-10782-3

[27] Dhineshbabu, N. R., & Bose, S. UV resistant and fire retardant properties in fabrics coated with polymer based nanocomposites derived from sustainable and natural resources for protective clothing application. Composites Part B: Engineering, 172, 555–563. (2019). https://doi.org/10.1016/j.compositesb.2019.05.013

[28] Ru, J., Hua, Y., Xu, C., Li, J., Li, Y., Wang, D., Gong, K., Wang, R., & Zhou, Z. Microwave-assisted preparation of submicron-sized FeTiO3 powders. Ceramics International, 40(5), 6799–6805, (2014). https://doi.org/10.1016/j.ceramint.2013.11.142

[29] Torres-Luna, J. A., Sanabria, N. R., & Carriazo, J. G. Powders of iron(III)-doped titanium dioxide obtained by direct way from a natural ilmenite. Powder Technology, 302, 254–260, (2016). https://doi.org/10.1016/j.powtec.2016.08.056

[30] Abdel Maksoud, M. I. A., Kassem, S. M., Ashour, A. H., & Awed, A. S. Recycled high-density polyethylene plastic reinforced with ilmenite as a sustainable radiation shielding material. RSC Advances, 13(30), 20698–20708, (2023). https://doi.org/10.1039/D3RA03757F

[31] Wijewardhana, T. Dilmi. U., & Ratnayake, A. S. Applicability of carbothermic reduction for upgrading Sri Lankan ilmenite ores: Towards converting ilmenite into synthetic rutile by mechanical activation. Bulletin of the National Research Centre, 45(1), 149, (2021). https://doi.org/10.1186/s42269-021-00608-9

[32] Guan, C., Yin, Z., Zhai, J., Hu, Y., Chen, P., & Sun, W. Surface modification of ilmenite by a novel surfactant dodecyliminodimethylenediphosphoinc acid and its sequent influence on ilmenite floatability. Separation Science and Technology, 55(2), 358–368. (2020). https://doi.org/10.1080/01496395.2019.1577270

[33] Chen, P., Chen, Y., Liu, H., Li, H., Chai, X., Lu, X., Sun, W., Wang, H., Luo, Y., & Wang, X. Novel Approach for Fine Ilmenite Flotation Using Hydrophobized Glass Bubbles as the Buoyant Carrier. Minerals, 11(3), 231, (2021). https://doi.org/10.3390/min11030231

[34] Wang, X., Shi, Z., Wang, J., Zhao, T., Ji, G., & Liu, L. Preparation, microstructure and dye adsorption behavior of nanostructured FeTiO3 with a magnetic recovery capacity. Functional Materials Letters, 13(03), 2051013, (2020). https://doi.org/10.1142/S1793604720510133

[35] Rajakaruna, T. P. B., Udawatte, C. P., Chandrajith, R., & Rajapakse, R. M. G. Nonhazardous Process for Extracting Pure Titanium Dioxide Nanorods from Geogenic Ilmenite. ACS Omega, 5(26), 16176–16182, (2020). https://doi.org/10.1021/acsomega.0c01756

[36] Jung, E. J., Kim, J., & Lee, Y. R. A comparative study on the chloride effectiveness of synthetic rutile and natural rutile manufactured from ilmenite ore. Scientific Reports, 11(1), 4045, (2021). https://doi.org/10.1038/s41598-021-83485-6

[37] Koochakzadeh, F., Norouzbeigi, R., & Shayesteh, H. Statistically optimized sequential hydrothermal route for FeTiO3 surface modification: Evaluation of hazardous cationic dyes adsorptive removal. Environmental Science and Pollution Research. (2022). https://doi.org/10.1007/s11356-022-23481-z

[38] Macías-Vargas, J.-A., Zanella, R., & Ramírez-Zamora, R.-M. Degradation of ciprofloxacin using a low-grade titanium ore, persulfate, and artificial sunlight. Environmental Science and Pollution Research, 27(23), 28623–28635, (2020). https://doi.org/10.1007/s11356-020-08293-3

[39] Silveira, J. E., Paz, W. S., Garcia-Muñoz, P., Zazo, J. A., & Casas, J. A. UV-LED/ilmenite/persulfate for azo dye mineralization: The role of sulfate in the catalyst deactivation. Applied Catalysis B: Environmental, 219, 314–321. (2017). https://doi.org/10.1016/j.apcatb.2017.07.072

[40] Tao, T., Glushenkov, A. M., Chen, Q., Hu, H., Zhou, D., Zhang, H., Boese, M., Liu, S., Amal, R., & Chen, Y. Porous TiO2 with a controllable bimodal pore size distribution from natural ilmenite. CrystEngComm, 13(5), 1322–1327, (2011). https://doi.org/10.1039/C0CE00533A

[41] Muzenda, C., Nkwachukwu, O. V., & Arotiba, O. A.. Synthetic Ilmenite (FeTiO3) Nanoparticles as a Heterogeneous Electro-Fenton Catalyst for the Degradation of Tetracycline in Wastewater. Industrial & Engineering Chemistry Research, 61(31), 11417–11428, (2022). https://doi.org/10.1021/acs.iecr.2c01464

[42] Thommes, M., Kaneko, K., Neimark, A. V., Olivier, J. P., Rodriguez-Reinoso, F., Rouquerol, J., & Sing, K. S. W. Physisorption of gases, with special reference to the evaluation of surface area and pore size distribution (IUPAC Technical Report). 87(9–10), 1051–1069, (2015). https://doi.org/10.1515/pac-2014-1117

[43] Tamura, H., Mita, K., Tanaka, A., Ito, M. Mechanism of Hydroxylation of Metal Oxide Surfaces. Journal of Colloid and Interface Science 243(1), 1 November 2001, 202-207, (2001). https://doi.org/10.1006/jcis.2001.7864